



OPEN ACCESS

EDITED BY

Francesco Del Galdo,
University of Leeds, United Kingdom

REVIEWED BY

Julie Worrell,
University of Glasgow,
United Kingdom
Steven O'Reilly,
STipe Therapeutics, Denmark

*CORRESPONDENCE

David Abraham
david.abraham@ucl.ac.uk
Jan-Willem Taanman
j.taanman@ucl.ac.uk

[†]These authors have contributed
equally to this work and share
first authorship

SPECIALTY SECTION

This article was submitted to
Autoimmune and Autoinflammatory
Disorders: Autoinflammatory
Disorders,
a section of the journal
Frontiers in Immunology

RECEIVED 27 July 2022

ACCEPTED 26 September 2022

PUBLISHED 11 October 2022

CITATION

Cantanhede IG, Liu H, Liu H,
Balbuena Rodriguez V, Shiwen X,
Ong VH, Denton CP, Ponticos M,
Xiong G, Lima-Filho JL, Abraham D,
Abu-Hanna J and Taanman J-W
(2022) Exploring metabolism in
scleroderma reveals opportunities for
pharmacological intervention for
therapy in fibrosis.
Front. Immunol. 13:1004949.
doi: 10.3389/fimmu.2022.1004949

COPYRIGHT

© 2022 Cantanhede, Liu, Liu,
Balbuena Rodriguez, Shiwen, Ong,
Denton, Ponticos, Xiong, Lima-Filho,
Abraham, Abu-Hanna and Taanman.
This is an open-access article
distributed under the terms of the
[Creative Commons Attribution License
\(CC BY\)](https://creativecommons.org/licenses/by/4.0/). The use, distribution or
reproduction in other forums is
permitted, provided the original
author(s) and the copyright owner(s)
are credited and that the original
publication in this journal is cited, in
accordance with accepted academic
practice. No use, distribution or
reproduction is permitted which does
not comply with these terms.

Exploring metabolism in scleroderma reveals opportunities for pharmacological intervention for therapy in fibrosis

Isabella Gomes Cantanhede^{1,2†}, Huan Liu^{1,3†}, Huan Liu¹,
Vestaen Balbuena Rodriguez¹, Xu Shiwen¹, Voo H. Ong¹,
Christopher P. Denton¹, Markella Ponticos¹, Guo Xiong³,
José Luiz Lima-Filho², David Abraham^{1*}, Jeries Abu-Hanna¹
and Jan-Willem Taanman^{4*}

¹Centre for Rheumatology and Connective Tissue Diseases, Division of Medicine, University College London, London, United Kingdom, ²Laboratory of Immunopathology Keizo Asami, Federal University of Pernambuco, Recife, Brazil, ³Health Science Center, Xi'an Jiaotong University, Xi'an, China, ⁴Department of Clinical and Movement Neurosciences, Queen Square Institute of Neurology, University College London, London, United Kingdom

Background: Recent evidence has indicated that alterations in energy metabolism play a critical role in the pathogenesis of fibrotic diseases. Studies have suggested that 'metabolic reprogramming' involving the glycolysis and oxidative phosphorylation (OXPHOS) in cells lead to an enhanced generation of energy and biosynthesis. The aim of this study was to assess the molecular basis of changes in fibrotic metabolism in systemic sclerosis (Scleroderma; SSc) and highlight the most appropriate targets for anti-fibrotic therapies.

Materials and methods: Dermal fibroblasts were isolated from five SSc patients and five healthy donors. Cells were cultured in medium with/without TGF- β 1 and with/without ALK5, pan-PIM or ATM kinase inhibitors. Extracellular flux analyses were performed to evaluate glycolytic and mitochondrial respiratory function. The mitochondrial network in TMRM-stained cells was visualized by confocal laser-scanning microscopy, followed by semi-automatic analysis on the ImageJ platform. Protein expression of ECM and fibroblast components, glycolytic enzymes, subunits of the five OXPHOS complexes, and dynamin-related GTPases and receptors involved in mitochondrial fission/fusion were assessed by western blotting.

Results: Enhanced mitochondrial respiration coupled to ATP production was observed in SSc fibroblasts at the expense of spare respiratory capacity. Although no difference was found in glycolysis when comparing SSc with healthy control fibroblasts, levels of phosphofructokinase-1 isoform PFKM were significantly lower in SSc fibroblasts ($P < 0.05$). Our results suggest that the

number of respirasomes is decreased in the SSc mitochondria; however, the organelles formed a hyperfused network, which is thought to increase mitochondrial ATP production through complementation. The increased mitochondrial fusion correlated with a change in expression levels of regulators of mitochondrial morphology, including decreased levels of DRP1, increased levels of MIEF2 and changes in OPA1 isoform ratios. TGF- β 1 treatment strongly stimulated glycolysis and mitochondrial respiration and induced the expression of fibrotic markers. The pan-PIM kinase inhibitor had no effect, whereas both ALK5 and ATM kinase inhibition abrogated TGF- β 1-mediated fibroblast activation, and upregulation of glycolysis and respiration.

Conclusions: Our data provide evidence for a novel mechanism(s) by which SSc fibroblasts exhibit altered metabolic programs and highlight changes in respiration and dysregulated mitochondrial morphology and function, which can be selectively targeted by small molecule kinase inhibitors.

KEYWORDS

fibrosis, glycolysis, kinase inhibitors, mitochondrial morphology, mitochondrial respiration, myofibroblasts, oxidative phosphorylation, systemic sclerosis

Introduction

Systemic sclerosis (scleroderma, SSc) is a rare immune-mediated inflammatory disease of unknown etiology (1, 2). One of the most characteristic pathological manifestations is the connective tissue fibrosis (3). This is especially marked in the diffuse cutaneous form of the disease, where overproduction of collagen and other extracellular matrix (ECM) proteins by connective tissue fibroblasts results in excessive ECM deposition. The fibroblasts are activated and differentiated into hyperproliferative myofibroblasts by growth factors and cytokines, such as transforming growth factor- β 1 (TGF- β 1). Progressive replacement of tissue architecture by the collagen-rich ECM results in a functional impairment of the affected organs. The fibrotic process is most prominent in the skin, lungs, gastrointestinal tract, heart, tendons and ligaments, and endocrine glands. Fibrotic damage to these organs accounts for much of the morbidity and mortality. Although clinical outcomes have improved, SSc is still considered incurable and difficult to treat (4).

There are two main biochemical pathways in the cell that generate metabolic energy in the form of ATP: glycolysis in the cytosol and oxidative phosphorylation in the mitochondria. Glycolysis converts glucose to pyruvate with the concomitant production of a small amount of ATP. Under aerobic conditions, pyruvate is imported into the mitochondria and further broken down in the tricarboxylic acid (TCA) cycle. Products of the TCA cycle (NADH, FADH₂) are subsequently oxidized, and the free energy of the redox reactions is used to sustain a proton

electrochemical gradient across the inner mitochondrial membrane, which is used to drive ATP synthesis (5). This process is called oxidative phosphorylation and is the main source of ATP in aerobic cells. It has been known for a long time that, unlike normal tissues, most cancers use glycolysis as main bioenergetic pathway to produce ATP, even in the presence of oxygen (6). This aerobic glycolysis is known as the Warburg effect and is thought to be important to increase anabolic metabolism (biosynthesis of building blocks) and resistance to apoptosis in hyperproliferative cancer cells (7, 8).

It is increasingly recognized that re-programming of cellular energy metabolism also occurs in fibrotic diseases (9). For instance, keloid “scar” fibroblasts, which share characteristics with fibroblasts from SSc patients, were reported to use glycolysis as their primary energy source (10). A switch to glycolysis was also found in lung tissue and myofibroblasts from patients with idiopathic pulmonary fibrosis (IPF) (11, 12). During early myofibroblast differentiation, the expression of the glycolytic enzymes hexokinase 2 (HK2), phosphofructokinase 1 and 6-phosphofructo-2-kinase/fructose-2,6-biphosphatase 3 (PFKFB3) were found to increase and remained high. Pharmacological inhibition of glycolysis, attenuated the profibrotic phenotype, suggesting that the increased glycolytic flux is essential for development of the fibrosis (12). In addition, alveolar type II cells in IPF patients were found to exhibit marked accumulation of dysfunctional mitochondria (13). Likewise, vascular pulmonary cells in patients with pulmonary arterial hypertension (PAH) showed mitochondrial abnormalities (14) and a shift towards glycolysis, which is likely to play a causal role in the deleterious vascular

remodeling because drug-induced reversal of the metabolic shift prevented remodeling (15). Similarly, differentiation of cultured hepatic stellate cells into myofibroblasts was shown to induce glycolysis (16). Finally, in mouse unilateral ureter obstruction-induced renal fibrosis and TGF- β 1-treated renal interstitial fibroblasts, high levels of glucose uptake, glycolytic enzymes and lactate production were observed. Pharmacological inhibition of pyruvate kinase type M2 (PKM2) phosphorylation at Tyr residue 105, which is known to suppress aerobic glycolysis, attenuated renal fibrosis and fibroblast activation (17).

As current treatments of SSc are limited and have substantial side effects, new insights into the pathological processes are needed to develop novel therapeutic approaches. We hypothesize that rewiring of the energy generating pathways contribute to the disease process of SSc to meet the increased demand of energy and anabolic metabolism for fibrogenesis. The aims of the current study were: (a) to investigate possible changes in energy metabolism in cell culture models of SSc, (b) to explore the molecular basis of these changes, and (c) to develop selective therapeutic strategies that target the disrupted metabolism and stop fibrosis.

Material and methods

Cell culturing

Primary dermal fibroblast cultures were established from skin explants of five early diffuse SSc patients (≤ 2 y from first non-Raynaud's symptom) and five unrelated, healthy, age-matched control subjects (Supplementary Table S1) according to standard procedures (18). From the patients, we took paired skin samples from lesional and uninvolved tissue. Donors provided prior informed written consent. Ethical approval was obtained from the Research Ethics Committee (reference: 6398) of the NHS Health Research Authority (NRES Committee London-Hampstead) in compliance with national legislation and the Declaration of Helsinki.

Cell passages at 3–7 were used for study. Cells were cultured in Dulbecco's modified Eagle medium (DMEM) containing GlutaMAX and 25 mM glucose (Gibco, ThermoFisher Scientific), supplemented with 10% fetal bovine serum (FBS), 1 mM sodium pyruvate, 50 units/ml of penicillin and 50 μ g/ml of streptomycin (culture medium) at 37°C in a humidified atmosphere of 5% CO₂ in air. For the experiments with TGF- β 1, cells were serum-starved in culture medium containing 0.1% FBS for 24 h before treatment with or without 2 ng/ml of TGF- β 1 (R&D Systems) and with or without 10 μ M SB431542 (Tocris Bioscience), 20 μ M AZD1208 (Tocris Bioscience) or 5 μ M KU55933 (Tocris Bioscience) for 24 h in fresh culture medium containing 0.1% FBS. Thousand-fold stock solutions were prepared in water (TGF- β 1) or dimethyl sulfoxide (small molecule inhibitors) and stored at -80°C. The concentration of

the inhibitors was informed by the literature and verified by viability assays using PrestoBlue Cell Viability Reagent (ThermoFisher Scientific), whereby only doses at which no toxic effects occurred were chosen.

Western blot analysis

For the study of α -smooth muscle actin (α -SMA) and ECM proteins, cell cultures were washed twice with cold phosphate-buffered saline (PBS) followed by extraction in cold RIPA buffer (Merck, Sigma-Aldrich), supplemented with Roche cOmplete Protease Inhibitor Cocktail (Merck, Sigma-Aldrich). Cell monolayers were collected with a cell scraper, centrifuged for 10 min at 16,000 \times g, 4°C, and supernatants were stored at -20°C for western blot analyses.

For the study of glycolytic pathway and mitochondrial proteins, cell cultures were washed with PBS and, subsequently, dislodged by trypsinization, collected by centrifugation, washed with PBS and extracted with 1% Triton X-100 in PBS, supplemented with protease inhibitors (1 μ M phenylmethylsulfonyl fluoride, 1 μ g/ml of pepstatin A and 1 μ g/ml of leupeptin) and Phosphatase Inhibitor Cocktail 2 and 3 (Merck, Sigma-Aldrich). After 15 min on ice, samples were centrifuged for 10 min at 16,000 \times g, 4°C, and the supernatants were stored at -80°C for western blot analyses.

Protein concentrations of the samples were determined with the Pierce BCA Protein Assay Kit (ThermoFisher Scientific) as detailed below. To prepare western blots, 10- μ g samples in 1 \times Laemmli Sample Buffer (BioRad) and 1 \times NuPAGE Sample Reducing Agent (ThermoFisher Scientific) were resolved on 4–20% or 7.5% Criterion TGX Stain-Free Precast Gels (BioRad) alongside SeeBlue Plus2 Pre-stained Protein (ThermoFisher Scientific) or Precision Plus Protein (BioRad) standards and blotted onto Trans-Blot Turbo 0.2- μ m PVDF membranes (BioRad) using a BioRad Trans-Blot Transfer System. Protein binding sites on the blots were saturated with 5% bovine serum albumin (BSA; for detection of phospho-proteins) or 10% skimmed milk powder (for detection of all other proteins) in PBS for 1 h, followed by a rinse with PBS, 0.3% Tween-20 and primary antibody incubation in PBS, 0.3% Tween-20, at 4°C, overnight. The primary antibodies are specified in Supplementary Table S2. Excess of primary antibodies was removed with three 10-min washes in PBS, 0.3% Tween-20, followed by a 1-h incubation with the appropriate horse radish peroxidase-conjugated secondary antibodies (Dako; P0160, P0447 and P0448) in PBS, 0.3% Tween-20, and another 3 washes. Blots were developed with Clarity Western ECL Substrate (BioRad). Capturing of the chemiluminescent signals was performed with a BioRad Chemidoc MP Imaging System. Signals were quantified with BioRad Image Lab 5.1 software. Afterwards, all blots were probed with an antibody against β -tubulin to verify loading. Antibody signals were normalized with

the aid of the anti- β -tubulin signal and expressed relative to the mean value of the control samples.

Extracellular flux analyses

Extracellular flux assays were performed on a Seahorse XFp platform (Agilent Technologies). To count the cells for seeding in the XFp cell culture microplates, they were dislodged by trypsinization, collected by centrifugation and resuspended in culture medium, followed by trypan blue exclusion cell counting on C-Chip Neubauer Improved Disposable Hemocytometer slides (NanoEnTek) in duplicate. Fibroblasts were seeded in wells of an XFp cell culture microplate at a density of 8,000 cells/well in 80 μ l of culture medium and cultured for 24 h. In the TGF- β 1 experiments, cells were serum-starved in the wells of the XFp cell culture microplate for a further 24 h prior to treatment with or without 2 ng/ml of TGF- β 1 and with or without 10 μ M SB431542, 20 μ M AZD1208 or 5 μ M KU55933 for 24 h in fresh culture medium containing 0.1% FBS.

To examine glycolytic function in glycolysis stress tests, the culture medium in the wells was replaced with 175 μ l XFp Base medium (Agilent Technologies) pH 7.0 (NaOH), containing 2 mM L-glutamine, with or without TGF- β 1 and with or without small molecule inhibitors. After 1 h of humidified incubation at 37°C, glycolysis was evaluated on the Seahorse platform. After three measurements under basal conditions, glucose was injected to a final concentration of 10 mM, followed by three measurements. Then, oligomycin A was injected to a final concentration of 1 μ M, followed by three measurements. Last of all, 2-deoxy-D-glucose was injected to a final concentration 50 mM, followed by three measurements. Glucose was prepared as a 2.5 M stock solution in water and stored at room temperature, while oligomycin A (Merck, Sigma-Aldrich) was prepared as a 10 mM stock solution in ethanol and 2-deoxy-D-glucose (Merck, Sigma-Aldrich) was prepared as a 500 mM stock solution in XFp Base medium pH 7.0 and both stored at -20°C.

To examine mitochondrial respiratory function in mitostress tests, the culture medium in the wells was replaced with 175 μ l XFp Base medium pH 7.0 (NaOH), containing 10 mM D-(+)-glucose, 1 mM sodium pyruvate and 2 mM L-glutamine, with or without TGF- β 1 and with or without small molecule inhibitors. After 1 h of humidified incubation at 37°C, respiration was assessed on the Seahorse platform. After three measurements under basal conditions, oligomycin A was injected to a final concentration of 1 μ M, followed by three measurements. Then, carbonyl cyanide 4-(trifluoromethoxy) phenylhydrazone (FCCP) was injected to a final concentration of 2 μ M, followed by three measurements. To finish, rotenone and antimycin A were injected, both at a final concentration of 1 μ M, followed by three measurements. Oligomycin A, FCCP, rotenone and antimycin A were purchased from Merck (Sigma-

Aldrich). They were prepared as 10 mM stock solutions in ethanol and stored at -20°C.

On each XFp cell culture plate, two different cultures were compared in triplicate, e.g., fibroblasts from a control subject and fibroblasts from a SSc patient, or fibroblasts from a SSc patient treated with vehicle and fibroblasts from the same SSc patient treated with TGF- β 1. All experiments were repeated independently 4 (Figure 8) or 6 (Figure 2) times by conducting two experiments per cell passage of two or three subsequent passages. Data were analyzed with Wave Desktop 2.6.1 software and a Microsoft Excel macro provided by Agilent Technologies. Results are expressed per cell number or amount of protein determined after the extracellular flux assay. Cell numbers in each well of the XFp cell culture plate were determined with the CyQUANT Cell Proliferation Assay Kit (ThermoFisher Scientific) by adding 220 μ l of CyQUANT GR dye/lysis solution to the aspirated wells, followed by mixing through pipetting up-and-down. Then, 200 μ l of the mixture was transferred to wells of a 96-well black plate with clear bottoms (Greiner). An empty row on the 96-well plate was filled with 200 μ l of a serial dilution of 0–25,000 cells in CyQUANT GR dye/lysis solution. The fluorescent signals were recorded at 480 nm excitation and 520 nm emission with a Synergy HT plate reader. In the TGF- β 1 experiments, the amount of protein in aspirated wells of the XFp cell culture plates were determined with the Pierce BCA Protein Assay Kit and a serial dilution of BSA. Standard curves for the number of cells *versus* the fluorescent signal or the concentration of BSA *versus* the absorption at 561 nm were constructed in Microsoft Excel. Equations of the standard curves were used to calculate the cell number or amount of protein per well.

Citrate synthase assays

The Triton X-100 extracts of the cell cultures prepared for western blot analyses were also used to determine citrate synthase activity. Assays were carried out in quadruplicate as described (19).

Mitochondrial network analysis

Cells were seeded at low density in 35-mm μ -dishes with a glass bottom (Ibidi). After 3–4 days of culturing, cells were rinsed with Hanks' balanced salt solution (HBSS; ThermoFisher Scientific), followed by incubation in 1 ml of 25 nM tetramethylrhodamine methyl ester (TMRM; Invitrogen, ThermoFisher Scientific) in HBSS. After 15 min of incubation, red fluorescent images (7 z-stacks of 0.15 μ m) were captured with a Nikon Eclipse Ti-E inverted confocal laser-scanning microscope, equipped with a \times 60 objective. Imaging data were

collected with NIS-Elements software (Nikon). Semi-automated analysis of mitochondrial networks in the cultured cells was performed with the MiNA macro toolset (20) on the FIJI distribution of the ImageJ platform (National Institutes of Health). All 15 different fibroblast cultures were analyzed; five cultures derived from control subjects, five cultures derived from uninvolved skin of SSc patients, and five cultures derived from involved skin of the same SSc patients. Six to 12 randomly chosen microscopic fields were studied of each culture with 1–10 cells per field. In total 17–58 cells of each culture were studied.

Statistical analyses

Graphs and statistical analyses were executed with GraphPad Prism software. Data are presented as mean \pm standard deviation. As the sample size was too small to confirm normal distribution, we used non-parametric Kruskal-Wallis tests to examine statistical significance. Mann-Whitney tests were used for pairwise comparisons. Statistical significance levels were set to $P < 0.05$ with Bonferroni correction for multiple pairwise comparisons.

Results

Expression levels of fibrotic markers

In this study, we compared paired fibroblasts cultures derived from uninvolved and lesional skin of five SSc patients with dermal fibroblast cultures derived from five control subjects. First, we investigated the expression levels of two

markers of fibrosis, α -smooth muscle actin (α -SMA) and collagen type 1 α 1 chain (COL-1) on western blots (Figure 1A). Compared to the control samples, α -SMA and COL-1 were clearly overexpressed in the uninvolved SSc samples. In the lesional SSc samples, the expression levels of α -SMA and COL-1 were even higher (Figures 1B, C). These results confirm the fibrotic phenotype of the SSc fibroblasts.

Glycolysis and mitochondrial respiration

To investigate whether energy metabolism in SSc fibroblasts is altered, we evaluated glycolysis and mitochondrial respiration with a Seahorse extracellular flux analyzer. We first determined the extracellular acidification rates (ECAR) as measure of glycolytic flux in glycolysis stress tests (Figure 2A). The experiments were repeated independently six times for each culture. The compiled data of the five pairs of SSc fibroblast cultures and five control cultures showed no differences in basal glycolysis, glycolytic capacity and glycolytic reserve (Figure 2B). Next, we determined the oxygen consumption rates (OCR) as measure of cellular respiration in mitostress tests (Figure 2C). Again, the experiments were repeated independently six times for each culture. The combined data for all 15 cultures revealed no differences in basal respiration and maximal respiration but indicated that the spare respiratory capacity was decreased in SSc fibroblasts, while the respiration coupled to ATP production was increased in SSc fibroblasts compared to the controls. Thus, the extracellular flux assays revealed a shift in mitochondrial respiration towards increased oxidative phosphorylation in SSc fibroblasts, while glycolytic flux did not change.

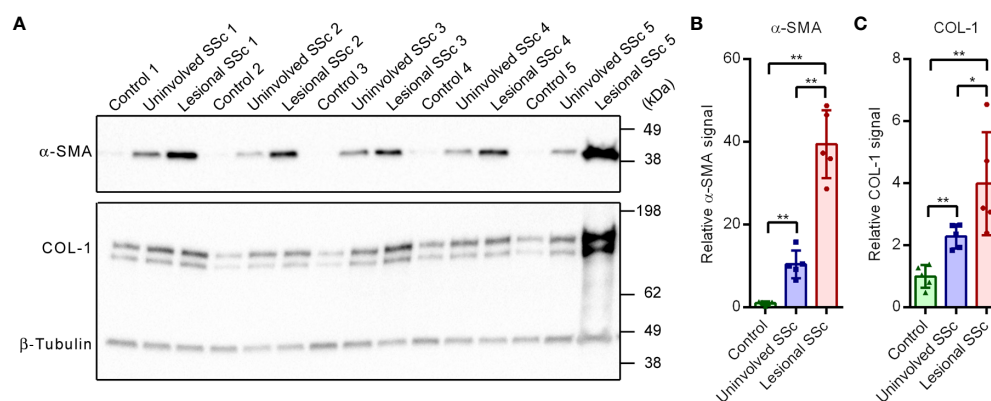
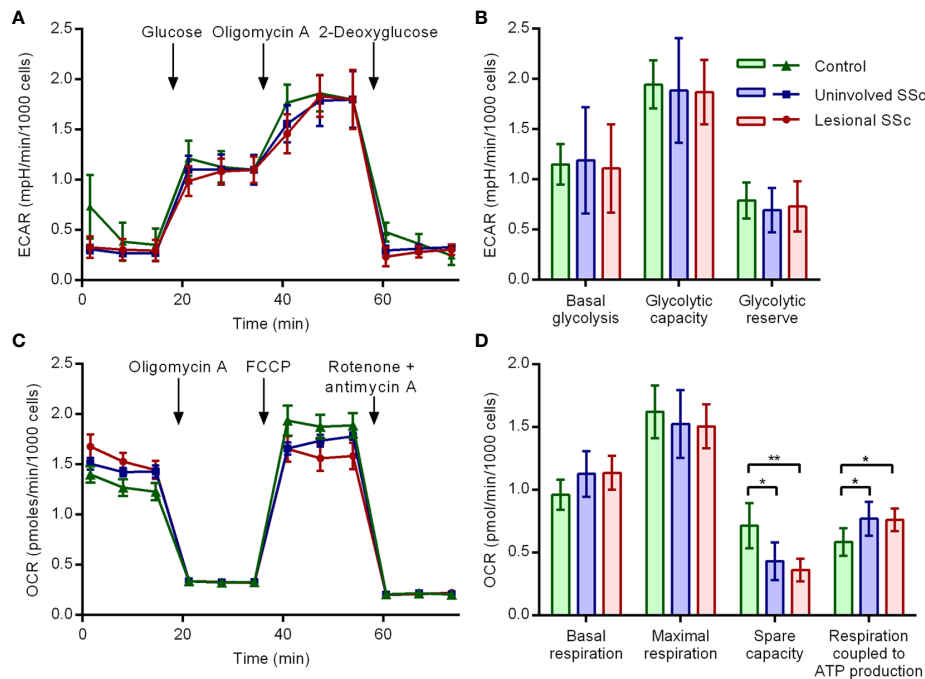


FIGURE 1

The fibrotic markers α -SMA and COL-1 are overexpressed in SSc fibroblasts. (A) Western blots with samples from five control, and five paired uninvolved and lesional SSc fibroblast cultures probed with antibodies against α -SMA, COL-1 and β -tubulin. Migration of protein standards is indicated. (B, C) Mean α -SMA and COL-1 signals, normalized for the β -tubulin signal and expressed relative to the mean value of the control samples. Data points show relative values of the individual samples. Error bars indicate standard deviations. Asterisks denote statistically significant differences ($*P < 0.05$, $**P < 0.01$).



Protein expression levels of enzymes of the glycolytic pathway and lactate secretion

Although the glycolytic stress tests did not suggest changes in glycolytic flux in the SSc fibroblasts, we investigated the glycolytic pathway and lactate secretion in more detail by looking at protein expression levels of key enzymes on western blots (Figure 3A). Hexokinase catalyzes the first step of glycolysis, the phosphorylation of glucose to glucose 6-phosphate (Supplementary Figure S1). The two most abundantly expressed isoenzymes HK1 and HK2 are critical for maintaining an elevated rate of glycolysis in cancer cells (21). Western blot analyses revealed no differences in HK1 and HK2 expression levels between control and SSc fibroblasts (Figures 3B, C).

Phosphofruktokinase 1 catalyzes the phosphorylation of fructose 6-phosphate to fructose 1,6-bisphosphate in the rate-limiting, third step of glycolysis (Supplementary Figure S1). The active tetrameric enzyme is comprised of different combinations of PFKL, PFKM and PFKP subunit isoforms (22, 23). The

western blots showed that levels of PFKL and PFKP were similar in control and SSc fibroblasts, but levels of PFKM were significantly lower in SSc samples compared to controls (Figures 3D–F).

The bifunctional 6-phosphofructo-2-kinase/fructose-2,6-bisphosphatase (PFKFB) catalyzes the synthesis and degradation of fructose 2,6-bisphosphate, thereby regulating its steady-state level (24). Fructose 2,6-bisphosphate is a positive allosteric regulator of phosphofruktokinase 1 (Supplementary Figure S1). Four different isoforms of PFKFB have been identified. Isoform PFKFB3, which is highly expressed in most cancers, is inducible by hypoxia and promotes glycolysis under hypoxic conditions (25, 26). Our western blots did not show significant differences of PFKFB3 levels between control and SSc fibroblasts (Figure 3G).

Glyceraldehyde-3-phosphate dehydrogenase (GAPDH) converts glyceraldehyde-3-phosphate to 1,3 bisphosphoglycerate during glycolysis (Supplementary Figure S1). GAPDH is considered to be a constitutively expressed housekeeping protein (27). In agreement with this, we found very similar GAPDH levels in the control and SSc samples on a western blot (Figure 3H).

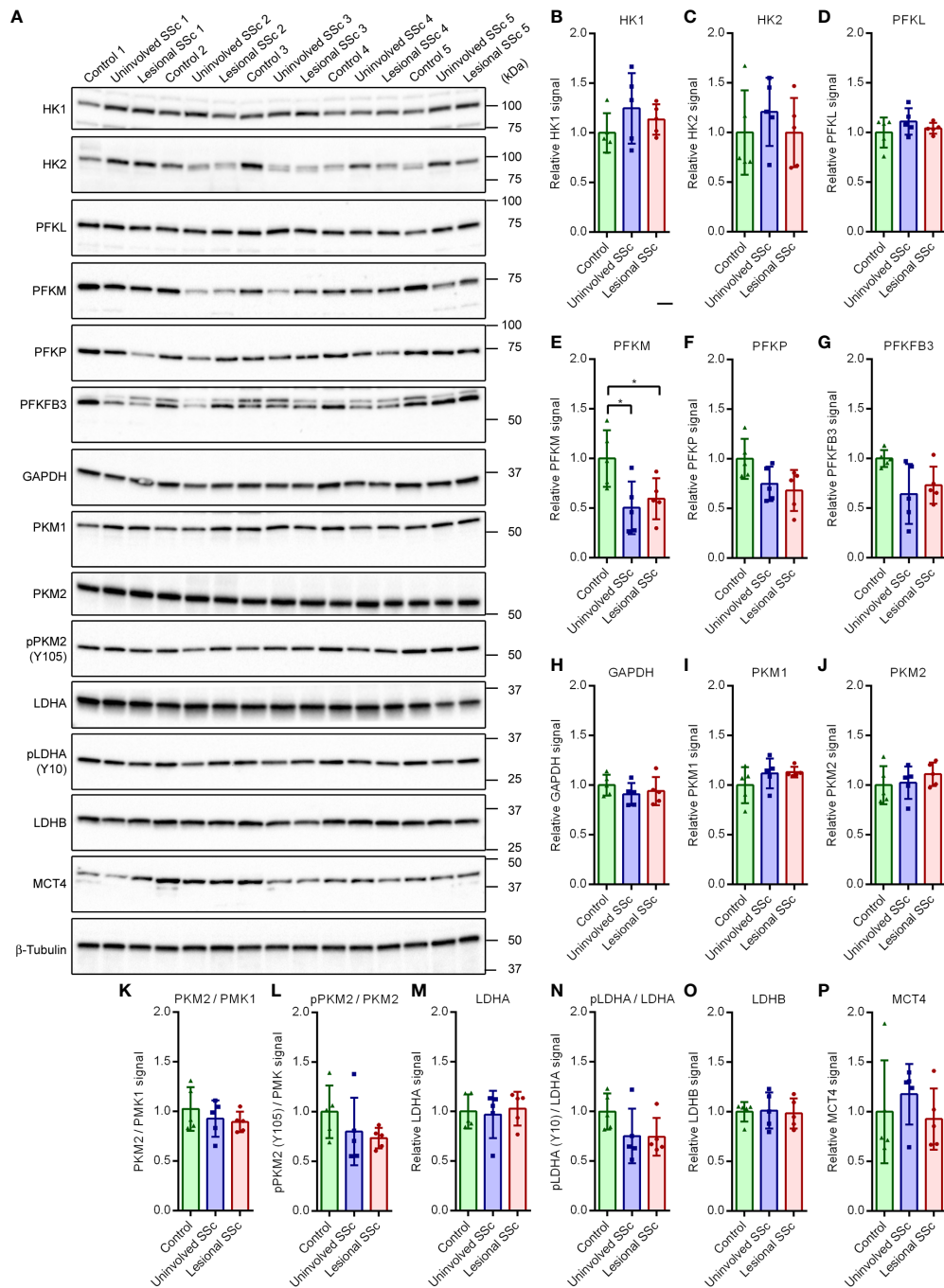


FIGURE 3

Muscle-type phosphofructokinase (PFKM) protein expression is decreased in SSc fibroblasts but the expression of other key enzymes of the glycolytic pathway and lactate secretion are unaffected. (A) Western blots with samples from five control, and five paired uninvolved and lesional SSc fibroblast cultures probed with antibodies against enzymes of the glycolytic pathway and lactate secretion as indicated. Blots were reprobbed with an antibody against β -tubulin to confirm even loading. Migration of protein standards is shown. (B–P) Mean signals of the indicated proteins or protein ratios, normalized for the β -tubulin signal and expressed relative to the mean value of the control samples. Data points show relative values of the individual samples. Error bars indicate standard deviations. Asterisks denote statistically significant differences ($*P < 0.05$).

Pyruvate kinase catalyzes the conversion of phosphoenolpyruvate to pyruvate in the terminal step of glycolysis (Supplementary Figure S1). Isoform PKM1 is expressed in most adult tissues, whereas isoform PKM2 is expressed during embryonic development and is the dominant isoform in tumors (28). PKM2 can switch from a dimeric, inactive to a tetrameric, active form. Formation of tetrameric PKM2 is inhibited by phosphorylation at Tyr residue 105 (pPKM2 (Y105)). Phosphorylation promotes aerobic glycolysis (29). Moreover, in response to glucose restriction, PKM2 translocates to the nucleus and acts as a transcriptional co-activator or protein kinase in cancer stem cells, modulating the metabolic flux (30, 31). Our western blots showed no differences in the expression levels of PKM1 and PKM2, the ratio of PKM2 *versus* PKM1, or the degree of phosphorylation of PKM2 between control and SSc samples (Figures 3I–L).

Lactate dehydrogenase catalyzes the reversible conversion of pyruvate and NADH to lactate and NAD⁺. Isoform LDHA possesses a higher affinity for pyruvate and preferentially converts pyruvate and NADH to lactate and NAD⁺. In contrast, isoform LDHB has a higher affinity for lactate and preferentially converts lactate and NAD⁺ to pyruvate and NADH (Supplementary Figure S1). LDHA phosphorylated at residue Tyr10 (pLDHA (Y10)) is found in a variety of human cancer cells. Phosphorylation enhances LDHA activity to promote aerobic glycolysis (32). On western blots we found similar expression levels of LDHA and LDHB, and the degree of phosphorylation of LDHA (Figures 3M–O).

Monocarboxylate transporters transfer lactate, pyruvate and other monocarboxylates across the plasma membrane. MCT4 facilitates the release of lactate from the cell (Supplementary Figure S1). Its expression is promoted by catabolic transcription factors, such as nuclear factor κ -light-chain-enhancer of activated B cells (NF- κ B) (33). Expression levels of MCT4 varied in the different cultures, but we did not detect significant differences between control and SSc fibroblasts on western blots (Figure 3P). Taken together, our western blot analysis of key enzymes of the glycolysis and lactate secretion revealed a decrease of PFKM protein expression levels in SSc fibroblasts compared to controls, but expression levels of other enzymes appeared unaffected.

Expression levels of subunits of the oxidative phosphorylation enzyme complexes

The mitostress tests demonstrated increased oxidative phosphorylation in the SSc fibroblasts. To investigate this further, we determined the expression levels of representative subunits of each of the five oxidative phosphorylation enzyme complexes on western blots (Figure 4A). The blots indicated that expression levels of subunit NDUF6 of Complex I were significantly decreased in SSc fibroblasts compared to controls (Figure 4B). Conversely,

expression levels of the SDHA subunit of complex II were comparable in SSc and control fibroblasts (Figure 4C). Parallel to NDUF6, however, the expression levels of the UQCRC2 subunit of Complex III and the MTCO1 subunit of Complex IV were decreased in SSc fibroblasts (Figures 4D, E). On the other hand, expression levels of the ATP5A subunit of Complex V showed no significant differences between SSc fibroblasts and controls (Figure 4F). Thus, our results suggest that the oxidative phosphorylation complexes I, III and IV that together form the respirasome supercomplex (34) are decreased in SSc fibroblasts, whereas levels of complexes II and V remain unchanged.

Citrate synthase activity

Citrate synthase is an enzyme of the mitochondrial TCA cycle (Supplementary Figure S1). Citrate synthase is commonly used as biomarker for mitochondrial density in cells (35–37). Although citrate synthase activity showed some variation in the different fibroblast cultures, we did not observe significant differences between SSc and control cells (Figure 4G).

Mitochondrial network morphology

The mitochondrial network in cells is continuously remodelled through fission and fusion events to adapt to changing physiological conditions (38). Mitochondrial fission generates new organelles and contributes to quality control by facilitating purging of damaged organelles *via* mitophagy. Mitochondrial fusion helps to mitigate stress through complementation of damaged mitochondria and is thought to increase mitochondrial ATP production. We investigated the mitochondrial network morphology in the SSc and control fibroblast cultures through live cell staining with the mitochondrial selective dye TMRM (Figure 5A). Analyses of the images revealed that there was no significant difference between the mitochondrial footprint per cell of SSc and control cultures; however, the mean length of the mitochondrial rods and branches, and the mean number of branches per mitochondrial network were increased in uninvolved SSc fibroblasts compared to controls. In the lesional SSc fibroblasts, these two parameters were still further increased (Figures 5B, C). These findings indicate that SSc fibroblasts have a hyperfused mitochondrial network.

Expression levels of proteins involved in mitochondrial fission and fusion

Mitochondrial network morphology is governed by the balance of mitochondrial fission and fusion events (39). To investigate how this balance is changed in SSc fibroblasts, we determined the

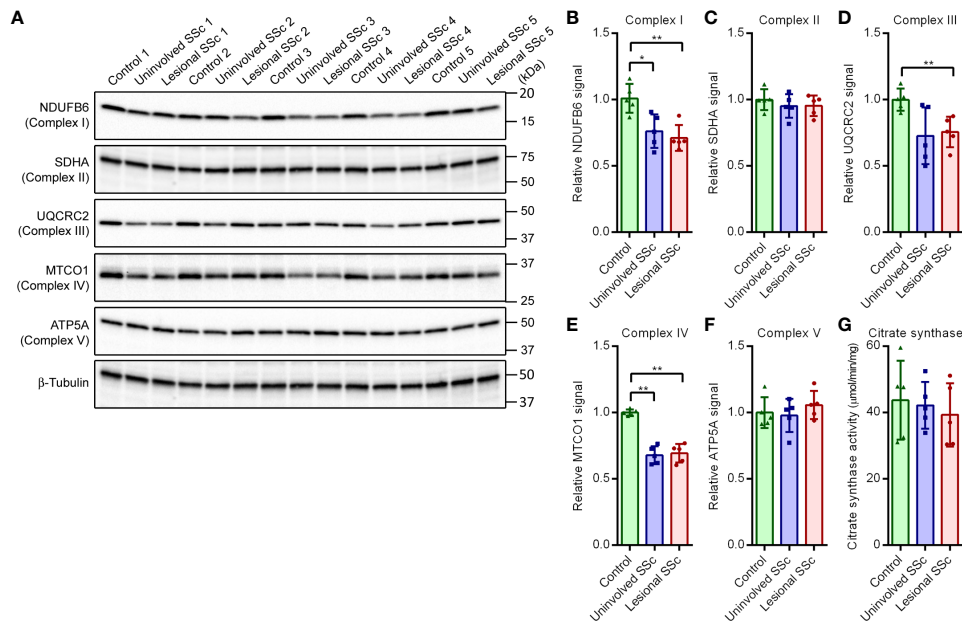


FIGURE 4

Subunits of OXPHOS enzyme complexes I, III and IV show decreased expression in SSc fibroblasts but subunits of OXPHOS enzyme complexes II and V, and citrate synthase activity are unaffected. **(A)** Western blots with samples from five control, and five paired uninvolved and lesional SSc fibroblast cultures probed with antibodies against subunits of the OXPHOS complexes as indicated. Blots were reprobed with an antibody against β -tubulin to confirm even loading. Migration of protein standards is shown. **(B–F)** Mean signals of the indicated proteins, normalized for the β -tubulin signal and expressed relative to the mean value of the control samples. Data points show relative values of the individual samples. **(G)** Mean citrate synthase activity of five control, and five paired uninvolved and lesional SSc fibroblast cultures. Data points show values of the individual samples. Error bars indicate standard deviations. Asterisks denote statistically significant differences (* $P < 0.05$, ** $P < 0.01$).

expression levels of dynamin-related GTPases and adaptors/receptors that mediate mitochondrial modelling ([Supplementary Figure S1](#)) by western blot analyses ([Figure 6A](#)). The GTPase DRP1 is a mainly cytosolic protein that plays a central role in

mitochondrial fission. Western blot analysis revealed that the expression levels of DRP1 were slightly, but statistically significant, lower in SSc fibroblasts compared to controls ([Figure 6B](#)). Phosphorylation of DRP1 at residue Ser616 (pDRP

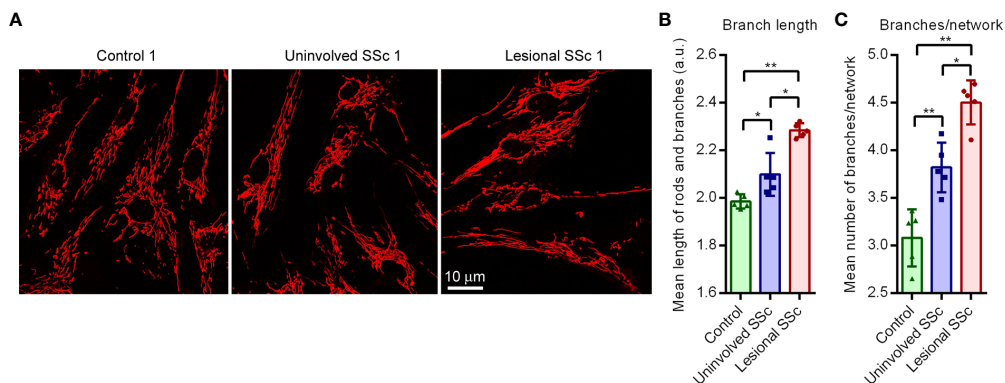


FIGURE 5

Cultured SSc fibroblasts have hyperfused mitochondrial networks. **(A)** Representative fluorescent micrographs of TMRM-stained control, uninvolved SSc and corresponding lesional SSc fibroblasts. **(B)** Mean length of mitochondrial rods and branches in arbitrary units (a.u.), and **(C)** mean number of branches per mitochondrial network in fibroblasts of five control and five paired uninvolved and lesional SSc cultures. Data point represent the mean length or the number of branches per network in 17–58 cells of the 15 individual cultures. Error bars indicate standard deviations. Asterisks denote statistically significant differences (* $P < 0.05$, ** $P < 0.01$).

(S616)) promotes mitochondrial fission (40), whereas phosphorylation of DRP1 at residue Ser637 (pDRP (S637)) promotes mitochondrial fusion (41, 42). Our western blots showed that the ratios of pDRP (S616) *versus* total DRP1 were similar in the control and SSc samples (Figure 6C). We did not detect pDRP1 (S637) on western blots, even after prolonged exposure (Supplementary Figure S2). The recruitment of cytosolic DRP1 to mitochondria is a key step in mitochondrial fission. MFF, and the paralogues MIEF1 (also known as MiD51 or SMCR7L) and MIEF2 (also known as MiD49 or SMCR7) are the receptor and adaptor proteins for DRP1 recruitment to the mitochondrial surface (43, 44). We found comparable expression levels of MIEF1 and MFF in control and SSc samples; however, expression levels of

MIEF2 were significantly higher in lesional SSc fibroblasts than in control fibroblasts (Figures 6D–F).

Fusion of the inner mitochondrial membrane is mediated by the GTPase OPA1, whereas fusion of the outer mitochondrial membrane is mediated by the GTPase paralogues MFN1 and MFN2 (39). Processing of so-called long OPA1 (L-OPA1) by multiple proteases generates short OPA1 (S-OPA1) forms (45). Fusion of the inner mitochondrial membrane depends on the equilibrium between L-OPA1 and S-OPA1. The western blots showed similar levels of MFN1 and MFN2 in control and SSc fibroblasts (Figures 6G, H). On the other hand, the ratios of L-OPA1 *versus* S-OPA1 were higher in the SSc samples than in the controls (Figure 6I). This may favor mitochondrial fusion.

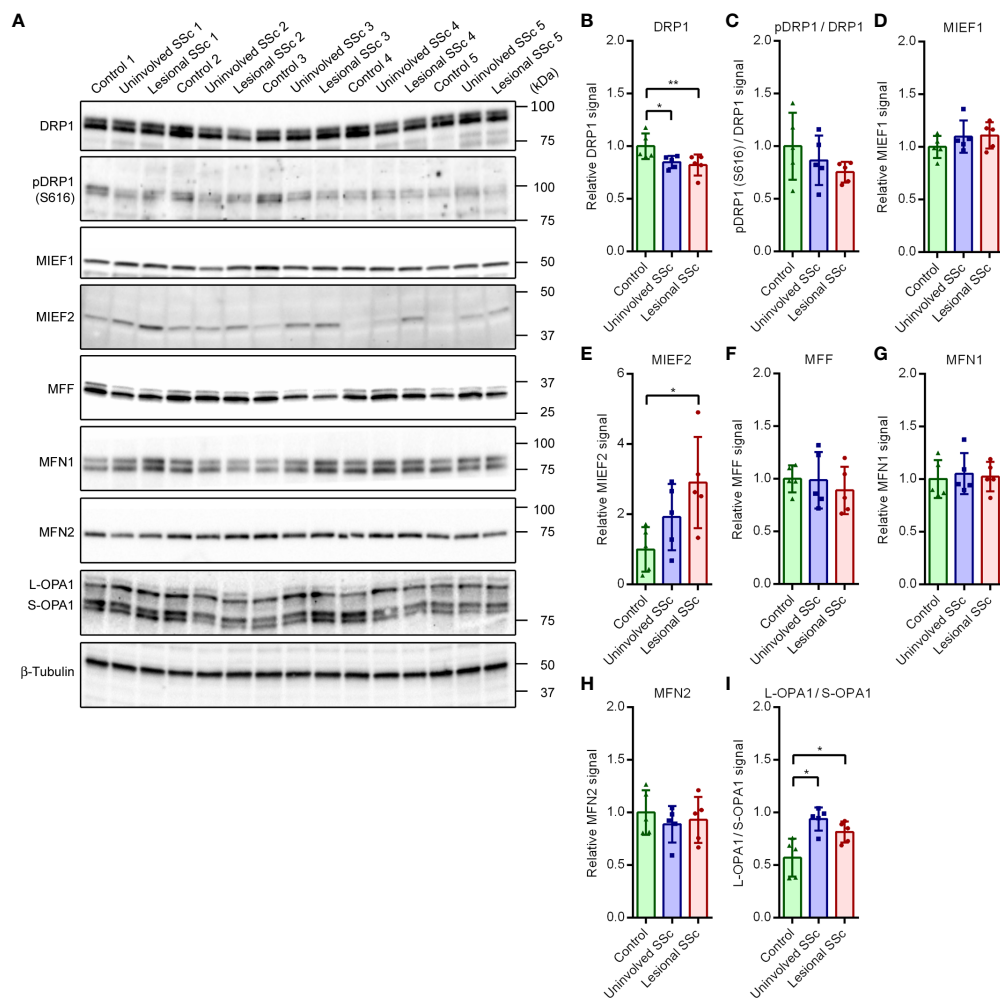


FIGURE 6

Expression of proteins engaged in mitochondrial fission and fusion shift in SSc fibroblasts to promote fusion. (A) Western blots with samples from five control, and five paired uninvolved and lesional SSc fibroblast cultures probed with antibodies against proteins involved in mitochondrial fission and fusion as indicated. Blots were re-probed with an antibody against β -tubulin to confirm even loading. Migration of protein standards is shown. (B–I) Mean signals of the indicated proteins, normalized for the β -tubulin signal and expressed relative to the mean value of the control samples or given as a ratio. Data points show relative values of the individual samples. Error bars indicate standard deviations. Asterisks denote statistically significant differences (* $P < 0.05$, ** $P < 0.01$).

Expression levels of fibrotic markers in TGF- β 1-activated fibroblasts treated with kinase inhibitors

When we compared the energy metabolism of SSc and healthy control fibroblasts, we observed no difference in glycolysis but noticed a small increase in respiration coupled to ATP production (Figure 2). To explore whether further induction of the fibrotic phenotype of SSc fibroblasts leads to additional increases in mitochondrial respiration and, possibly, glycolysis, cultures were treated with TGF- β 1. This cytokine is a well-known activator of fibrotic genes and has long been implicated in the pathogenesis of SSc (46). In addition, we tested whether three small molecule kinase inhibitors, SB431542, AZD1208 and KU55933, were able to reverse the effects of TGF- β 1 treatment. SB431542 is a specific inhibitor of the TGF- β 1 activin receptor-like kinase (ALK)-4, -5 and -7 (47). AZD1208 is a specific inhibitor of Proviral Integration site for Moloney murine leukemia virus (PIM) kinase-1, -2 and -3 (48). KU55933 is a selective Ataxia-Telangiectasia Mutated (ATM) kinase inhibitor (49). These inhibitors are known to suppress matrix production, modulate cell proliferation and regulate differentiation programs (50–52).

First, we investigated the effect of TGF- β 1 and the three kinase inhibitors on the expression levels of the fibrotic markers fibronectin, Col-1, α -SMA, and Connective Tissue Growth Factor (CTGF) in lesional SSc and control fibroblast cultures. Western blots showed that TGF- β 1 treatment markedly induced the expression levels of the four fibrotic markers in both cell types (Figure 7). Treatment with SB431542 completely prevented the increase in expression of the fibrotic markers in TGF- β 1-treated

cells (Figure 7A; Supplementary Figures S3A–D). AZD1208 treatment, in contrast, had no effect on the expression levels of the fibrotic markers (Figure 7B; Supplementary Figures S3E–H), whereas KU55933 prevented the TGF- β 1-induced expression of COL-1, α -SMA and CTGF in control and lesional fibroblasts (Figure 7C; Supplementary Figures S3I–L).

Glycolysis and mitochondrial respiration in TGF- β 1-activated lesional SSc fibroblasts treated with kinase inhibitors

Finally, we studied of effects of TGF- β 1 activation with or without SB431542, AZD1208 or KU55933 treatment on energy metabolism in lesional SSc fibroblast cultures. We first performed glycolytic stress tests on the Seahorse platform (Figure 8A). The combined results of four different lesional SSc cultures demonstrated that TGF- β 1 activation tripled the basal glycolysis as well as the glycolytic capacity (Figure 8B). SB431542 and KU55933 treatment counteracted the glycolytic stimulation of TGF- β 1 but AZD1208 treatment had no significant effect. We then carried out mitostress tests to assess mitochondrial respiration (Figure 8C). The compiled data of four different lesional SSc cultures indicated that basal respiration and respiration coupled to ATP production quadrupled after TGF- β 1 activation, while maximal respiration more than doubled and spare respiratory capacity increased by about half (Figure 8D). SB431542 treatment prevented the stimulatory effects of TGF- β 1 on basal and maximal respiration, and respiration coupled to ATP production. AZD1208 treatment had no significant effect on TGF- β 1-

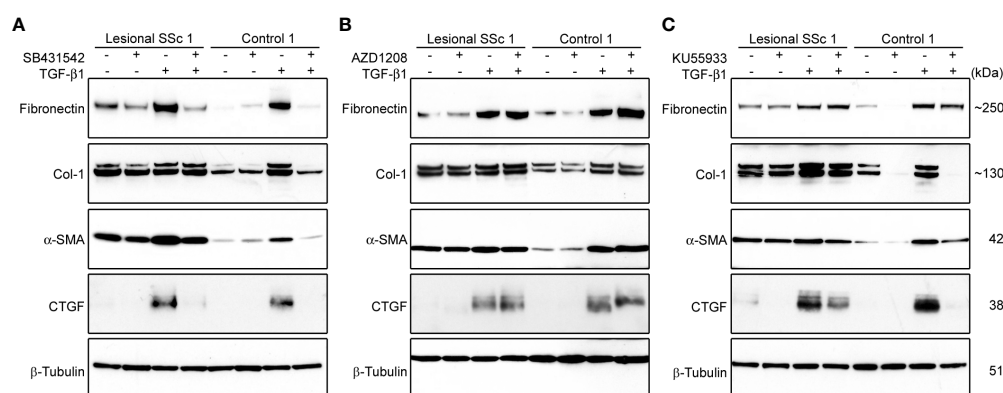


FIGURE 7

The kinase inhibitors SB431542 and KU55933, but not AZD1208, prevent TGF- β 1-induced overexpression of α -SMA and ECM proteins in lesional SSc and control fibroblasts. (A–C) Western blots with samples from a lesional SSc and a control fibroblast culture treated vehicle or 2 ng/ml of TGF- β 1 and/or 10 μ M SB431542, 20 μ M AZD1208 or 5 μ M KU55933, and probed with antibodies against α -SMA or ECM proteins as indicated. Blots were reprobbed with an antibody against β -tubulin to verify even loading.

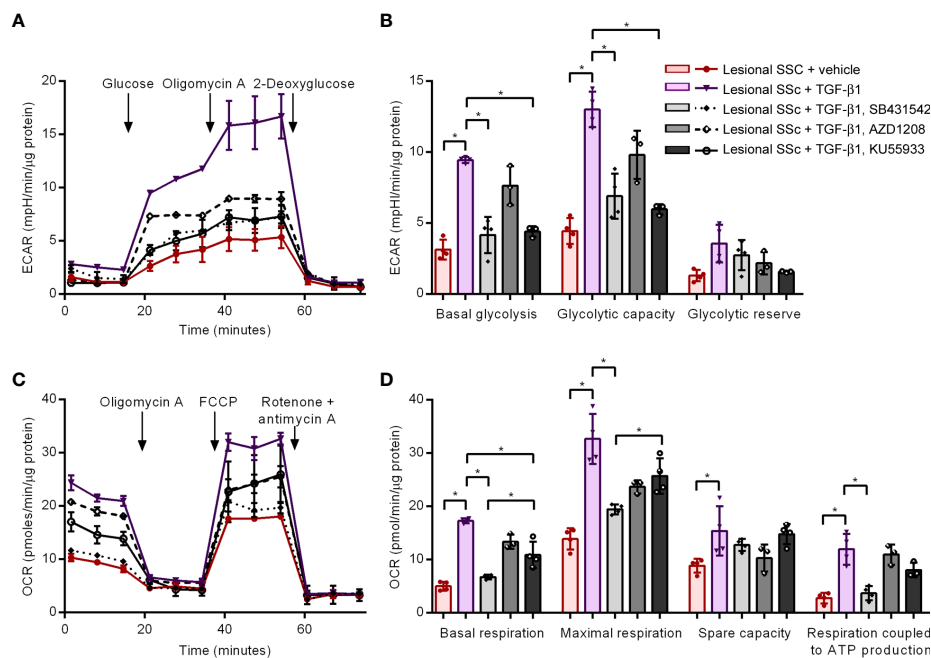


FIGURE 8

The kinase inhibitors SB431542 and KU55933, but not AZD1208, prevent TGF- β 1-induced increases in glycolysis and mitochondrial respiration in lesional SSC fibroblasts. (A) Extracellular acidification rates (ECAR) in representative glycolysis stress tests of a lesional SSC fibroblast culture treated vehicle or 2 ng/ml of TGF- β 1 with or without 10 μ M SB431542, 20 μ M AZD1208 or 5 μ M KU55933. Glucose, oligomycin A and 2-deoxyglucose were sequentially added to delineate glycolytic function. Error bars indicate standard deviation of technical triplicates. (B) Mean basal glycolysis, glycolytic capacity and glycolytic reserve of four lesional SSC fibroblast cultures treated vehicle or 2 ng/ml of TGF- β 1 with or without 10 μ M SB431542, 20 μ M AZD1208 or 5 μ M KU55933. Error bars indicate standard deviation. (C) Oxygen consumption rates (OCR) in representative mitostress tests of a lesional SSC fibroblast culture treated vehicle or 2 ng/ml of TGF- β 1 with or without 10 μ M SB431542, 20 μ M AZD1208 or 5 μ M KU55933. Oligomycin A, FCCP and rotenone + antimycin A were sequentially added to delineate mitochondrial respiratory function. Error bars indicate standard deviation of technical triplicates. (D) Mean basal respiration, maximal respiration, spare respiratory capacity and respiration coupled to ATP production of four lesional SSC fibroblast cultures treated vehicle or 2 ng/ml of TGF- β 1 with or without 10 μ M SB431542, 20 μ M AZD1208 or 5 μ M KU55933. Error bars indicate standard deviation. Asterisks denote statistically significant differences (* P <0.05).

stimulated respiration. KU55933 treatment significantly reduced the TGF- β 1-stimulated basal respiration but not as potent as SB431542.

Discussion

The objective of this study was to investigate the remodeling of energy metabolism in cell culture models of SSC in order to develop therapeutic strategies that target the disrupted metabolism and reverse the fibrotic phenotype. Although metabolic remodeling has been documented in other fibrotic diseases, studies of the role of energy metabolism in SSC are limited (53, 54). First, we compared paired fibroblasts cultures derived from uninvolved and lesional skin of five SSC patients with dermal fibroblast cultures from five control subjects. Western blot analyses for the fibrotic markers α -SMA and COL-1 confirmed the fibrotic phenotype of SSC fibroblasts. Glycolytic stress tests did not reveal differences in glycolysis

between SSC and control cultures. It is of course possible that our experiments are underpowered and that a larger number of patient and control samples would reveal a difference. The mitostress tests, however, exposed a small but significant increase in mitochondrial respiration coupled to ATP production at the expense of the spare respiratory capacity. These results suggest that SSC fibroblasts boost their oxidative phosphorylation to meet the increased bioenergetic demand of enhanced ECM protein synthesis and proliferation.

Assessment of the expression levels of key, rate-limiting enzymes of the glycolytic pathway and lactate secretion on western blots showed that levels of the phosphofructokinase 1 isoform PFKM were significantly lower in SSC fibroblasts compared to control fibroblasts, while levels of the isoforms PFKL and PFKP were unaffected. Of the three isoforms, PFKM has the highest affinities for fructose 6-phosphate and ATP. In addition, PFKM is the least sensitive to fructose 2,6-bisphosphate allosteric modulation and ATP inhibition (23). In other words, PFKM is the most active enzyme but is less

adaptable than PFKL and PFKP. Therefore, the lower PFKM expression suggests that glycolytic regulation may be of greater importance than activity for SSc fibroblast.

We also determined the expression levels of representative subunits of each of the five oxidative phosphorylation enzyme complexes by western blotting. Our results indicated that subunits of the oxidative phosphorylation complexes I, III and IV are decreased by ~25% in SSc fibroblasts compared to control samples, whereas levels of complexes II and V remain unchanged. The mitochondrial footprint and the activity of the TCA cycle enzyme citrate synthase in SSc fibroblasts corresponded to that of controls, suggesting that the mitochondrial mass in the cells is unaffected. Complexes I, III and IV form a supercomplex called the respirasome (34). When taken together, our results suggest that the number of respirasomes decrease in mitochondria of SSc fibroblasts. This is an unexpected finding because basal respiration and respiratory capacity did not change in SSc fibroblasts. Possibly, post-transcriptional modifications of the respirasome modulate its activity to increase coupling to ATP production. Mitochondrial morphology is controlled by energy metabolism. Live cell staining of the mitochondrial network demonstrated that SSc fibroblasts have a hyperfused network. Mitochondrial fusion is known to be driven by bioenergetic demand and stress (38). Fusion of mitochondria is thought to increase mitochondrial ATP production through complementation. Thus, the mitochondrial hyperfusion in SSc fibroblasts may promote respiration coupled to ATP production, reflecting the increased bioenergetic demand of the cells.

When we investigated the molecular basis of mitochondrial hyperfusion in SSc fibroblasts by western blot analyses of proteins involved in mitochondrial modelling, we found that the fission promoting protein DRP1 was decreased in SSc fibroblasts compared to controls; however, we did not find changes in the level of post-transcriptional phosphorylation of DRP1. As the phosphorylation determines the activity of DRP1 (55), the decreased levels of total DRP1 in SSc fibroblasts do not explain the mitochondrial hyperfusion in these cells. The western blots also revealed that MIEF2 was increased in SSc fibroblasts. MIEF2 acts as an adaptor of DRP1 and its receptor MFF, linking DRP1 with MFF on the mitochondrial surface (44). The higher levels of MIEF2 may recruit inactive DRP1 to the mitochondrial surface resulting in mitochondrial elongation (56). Alternatively, the upregulation of MIEF2 may sequester DRP1 in DRP1-MIEF2-MFF as well as DRP1-MIEF2 complexes, inhibiting direct interaction between DRP1 and MFF and resulting in mitochondrial fusion (57). In addition, western blot analyses indicated that the ratio of L-OPA1 *versus* S-OPA1 were higher in SSc fibroblasts than in the control cells. The inner mitochondrial membrane embedded protein L-OPA1 is processed by multiple proteases to S-OPA proteins that have

lost their membrane spanning N-terminus. Fusion of the inner membrane is determined by the balance between L-OPA1 and S-OPA1 (39). The observed shift towards L-OPA in SSc fibroblasts may favor mitochondrial fusion.

In the final experiments, we compared lesional SSc fibroblasts with their TGF- β 1-induced myofibroblast derivatives to mimic a more advanced stage of fibrosis. Western blot analyses for the fibrotic markers CTGF, α -SMA, COL-1 and fibronectin demonstrated that TGF- β 1 treatment induced the expression of all four fibrotic markers, confirming myofibroblast differentiation. To dissect the key signaling pathways in addition to determining the role of classical TGF- β 1 signaling (*via* the kinase ALK5), we also explored the role of two other pathways regulated by PIM kinase (58) and ATM kinase (59) that have been shown to have a role in fibrosis. Co-treatment with the TGF- β 1 receptor/ALK5 inhibitor SB431542 completely prevented the TGF- β 1-induced expression of the fibrotic markers, whereas co-treatment with the pan-PIM kinase inhibitor AZ1208 was ineffective. Co-treatment with the ATM kinase inhibitor KU55933 prevented the TGF- β 1-induced expression of COL-1, α -SMA and CTGF. Glycolytic and mitostress tests demonstrated that TGF- β 1 robustly stimulated basal glycolysis and glycolytic capacity, as well as basal and maximal respiration, and respiration coupled to ATP production. TGF- β 1-mediated stimulation of glycolysis and glutaminolysis, but not of mitochondrial respiration, was reported in normal human dermal fibroblasts by Henderson et al. (60). However, Bernard et al. (61, 62) and Bates et al. (63) reported a TGF- β 1-mediated stimulation of glycolysis and mitochondrial respiration in normal human lung fibroblasts and human primary hepatic stellate cells, respectively. In addition, increased mitochondrial respiration and content has been documented during TGF- β 1-mediated differentiation of NIH/3T3 mouse fibroblasts (64) and an upregulation of mitochondrial mass has been reported in TGF- β 1-treated normal human lung fibroblasts (65). Thus, our results with SSc dermal fibroblasts are generally supported by findings in other laboratories. Interestingly, co-treatment with SB431542 and KU55933 neutralized the TGF- β 1-mediated stimulation of glycolysis and mitochondrial respiration, but AZD1208 treatment had no significant effect. The differential impact of TGF- β 1 signaling *via* the canonical Smad pathway, and the PIM and ATM kinase on fibroblast energy generation highlights additional pathways to those previously identified (mTOR/AMPK/p38) as potentially critical to fibroblast metabolism underpinning scarring and fibrosis (61, 66, 67). The interaction(s) between these pathways and the mechanisms involved leading to fibrogenesis are being actively studied and once fully elucidated will allow identification of new markers and crucial candidates for the management and treatment of tissue fibrosis.

Data availability statement

The raw data supporting the conclusions of this article will be made available by the authors, without undue reservation.

Ethics statement

This study was reviewed and approved by Research Ethics Committee (reference: 6398) of the NHS Health Research Authority (NRES Committee London-Hampstead). The patients/participants provided their written informed consent to participate in this study.

Author contributions

Conception and design: DA, JA-H and J-WT. Provision of patients: VO and CD. Collection and preservation of cell cultures: XS. Collection and analysis of results: IC, HL (Xi'an), HL (UCL), VR and JWT. Drafting of manuscript and preparation of figures: J-WT. Editing of manuscript: MP, GX, JL-F, JA-H, DA and J-WT. All authors contributed to the article and approved the submitted version.

Funding

IC was supported by the Conselho Nacional de Desenvolvimento Científico e Tecnológico and Ciência Sem Fronteiras, Brazil. HL (Xi'an) was a recipient of a University Graduate Students Studying Abroad awarded from the Chinese Scholarship Council. HL (UCL) was awarded a Wellcome Trust Biomedical Vacation Scholarship (code: 213295/Z/18/Z). DA obtained funding from Versus Arthritis (formerly Arthritis

Research UK; codes: 21810 and 19427), the Royal Free Charity (Fund 97), Scleroderma and Raynaud's UK, and The Rosetrees Trust (code: M96-F1/F2). J-WT obtained funding from the Royal Free Charity (Fund 42).

Acknowledgments

We acknowledge the support from Ms Korsia Khan and Ms Bahja Ahmed Abdi for laboratory management, and Dr Ioannis Papaioannou for technical expertise.

Conflict of interest

The authors declare that the research was conducted in the absence of any commercial or financial relationships that could be construed as a potential conflict of interest.

Publisher's note

All claims expressed in this article are solely those of the authors and do not necessarily represent those of their affiliated organizations, or those of the publisher, the editors and the reviewers. Any product that may be evaluated in this article, or claim that may be made by its manufacturer, is not guaranteed or endorsed by the publisher.

Supplementary material

The Supplementary Material for this article can be found online at: <https://www.frontiersin.org/articles/10.3389/fimmu.2022.1004949/full#supplementary-material>

References

- Allanore Y, Simms R, Distler O, Trojanowska M, Pope J, Denton CP, et al. Systemic sclerosis. *Nat Rev Dis Primer* (2015) 1:1. doi: 10.1038/nrdp.2015.2
- Denton CP, Khanna D. Systemic sclerosis. *Lancet* (2017) 390:1685–99. doi: 10.1016/S0140-6736(17)30933-9
- Varga J, Abraham D. Systemic sclerosis: A prototypic multisystem fibrotic disorder. *J Clin Invest* (2007) 117:557–67. doi: 10.1172/JCI31139
- Denton CP, Ong VH. Targeted therapies for systemic sclerosis. *Nat Rev Rheumatol* (2013) 9:451–64. doi: 10.1038/nrrheum.2013.46
- Vercellino I, Sazanov LA. The assembly, regulation and function of the mitochondrial respiratory chain. *Annu Rev Cell Dev Biol* (2022) 23:141–61. doi: 10.1038/s41580-021-00415-0
- Warburg O, Wind F, Negelein E. The metabolism of tumors in the body. *J Gen Physiol* (1927) 8:519–30. doi: 10.1085/jgp.8.6.519
- Lunt SY, vander Heiden MG. Aerobic glycolysis: Meeting the metabolic requirements of cell proliferation. *Annu Rev Cell Dev Biol* (2011) 27:441–64. doi: 10.1146/annurev-cellbio-092910-154237
- Huber HJ, Dussmann H, Kilbride SM, Rehm M, Prehn JHM. Glucose metabolism determines resistance of cancer cells to bioenergetic crisis after cytochrome-c release. *Mol Syst Biol* (2011) 7:470. doi: 10.1038/msb.2011.2
- Henderson J, O'Reilly S. The emerging role of metabolism in fibrosis. *Trends Endocrinol Metab* (2021) 32:639–53. doi: 10.1016/j.tem.2021.05.003
- Vincent AS, Phan TT, Mukhopadhyay A, Lim HY, Halliwell B, Wong KP. Human skin keloid fibroblasts display bioenergetics of cancer cells. *J Invest Dermatol* (2008) 128:702–9. doi: 10.1038/sj.jid.5701107
- Kottmann RM, Kulkarni AA, Smolnycki KA, Lyda E, Dahanayake T, Salibi R, et al. Lactic acid is elevated in idiopathic pulmonary fibrosis and induces myofibroblast differentiation via pH-dependent activation of transforming growth factor- β . *Am J Respir Crit Care Med* (2012) 186:740–51. doi: 10.1164/rccm.201201-0084OC
- Xie N, Tan Z, Banerjee S, Cui H, Ge J, Liu R-M, et al. Glycolytic reprogramming in myofibroblast differentiation and lung fibrosis. *Am J Respir Crit Care Med* (2015) 192:1462–74. doi: 10.1164/rccm.201504-0780OC

13. Bueno M, Lai YC, Romero Y, Brands J, St Croix CM, Kamga C, et al. PINK1 deficiency impairs mitochondrial homeostasis and promotes lung fibrosis. *J Clin Invest* (2015) 125:521–38. doi: 10.1172/JCI74942
14. Ryan J, Dasgupta A, Huston J, Chen KH, Archer SL. Mitochondrial dynamics in pulmonary arterial hypertension. *J Mol Med (Berl)* (2015) 93:229–42. doi: 10.1007/s00109-015-1263-5
15. Sutendra G, Bonnet S, Rochefort G, Haromy A, Folmes KD, Lopaschuk GD, et al. Fatty acid oxidation and malonyl-CoA decarboxylase in the vascular remodeling of pulmonary hypertension. *Sci Transl Med* (2010) 2:44ra58. doi: 10.1126/scitranslmed.3001327
16. Chen Y, Choi SS, Michelotti GA, Chan IS, Swiderska-Syn M, Karaca GF, et al. Hedgehog controls hepatic stellate cell fate by regulating metabolism. *Gastroenterology* (2012) 143:1319–29. doi: 10.1053/j.gastro.2012.07.115
17. Ding H, Jiang L, Xu J, Bai F, Zhou Y, Yuan Q, et al. Inhibiting aerobic glycolysis suppresses renal interstitial fibroblast activation and renal fibrosis. *Am J Physiol Renal Physiol* (2017) 313:F561–75. doi: 10.1152/ajprenal.00036.2017
18. Park IH, Lerou PH, Zhao R, Huo H, Daley GQ. Generation of human-induced pluripotent stem cells. *Nat Protoc* (2008) 3:1180–6. doi: 10.1038/nprot.2008.92
19. Protasoni M, Kroon AM, Taanman JW. Mitochondria as oncotarget: a comparison between the tetracycline analogs doxycycline and COL-3. *Oncotarget* (2018) 9:33818–31. doi: 10.18632/oncotarget.26107
20. Valente JA, Maddalena LA, Robb EL, Moradi F, Stuart JA. A simple ImageJ macro tool for analyzing mitochondrial network morphology in mammalian cell culture. *Acta Histochem* (2017) 119:315–26. doi: 10.1016/j.acthis.2017.03.001
21. Smith TA. Mammalian hexokinases and their abnormal expression in cancer. *Br J BioMed Sci* (2000) 57:170–8.
22. Vora S, Seaman C, Durham S, Piomelli S. Isozymes of human phosphofructokinase: identification and subunit structural characterization of a new system. *Proc Natl Acad Sci USA* (1980) 77:62–6. doi: 10.1073/pnas.77.1.62
23. Fernandes PM, Kinkead J, McNaie I, Michels PAM, Walkinshaw MD, Fernandes PM, et al. Biochemical and transcript level differences between the three human phosphofructokinases show optimization of each isoform for specific metabolic niches. *Biochem J* (2020) 477:4425–41. doi: 10.1042/BCJ20200656
24. Rider MH, Bertrand L, Vertommen D, Michels PA, Rousseau GG, Hue L. 6-phosphofructo-2-kinase/fructose-2,6-bisphosphatase: head-to-head with a bifunctional enzyme that controls glycolysis. *Biochem J* (2004) 381:561–79. doi: 10.1042/BJ20040752
25. Atsumi T, Chesney J, Metz C, Leng L, Donnelly S, Makita Z, et al. High expression of inducible 6-phosphofructo-2-kinase/fructose-2,6-bisphosphatase (iPFK-2; PFKFB3) in human cancers. *Cancer Res* (2002) 62:5881–7.
26. Yi M M, Ban Y, Tan Y, Xiong W, Li G, Xiang B. 6-Phosphofructo-2-kinase/fructose-2,6-bisphosphatase 3 and 4: A pair of valves for fine-tuning of glucose metabolism in human cancer. *Mol Metab* (2019) 20:1–13. doi: 10.1016/j.molmet.2018.11.013
27. Barber RD, Harmer DW, Coleman RA, Clark BJ. GAPDH as a housekeeping gene: analysis of GAPDH mRNA expression in a panel of 72 human tissues. *Physiol Genomics* (2005) 21:389–95. doi: 10.1152/physiolgenomics.00025.2005
28. Christofk HR, Vander Heiden MG, Harris MH, Ramanathan A, Gerszten RE, Wei R, et al. The M2 splice isoform of pyruvate kinase is important for cancer metabolism and tumour growth. *Nature* (2008) 452:230–3. doi: 10.1038/nature06734
29. Hitosugi T, Kang S, Vander Heiden MG, Chung T-W, Elf S, Lythgoe K, et al. Tyrosine phosphorylation inhibits PKM2 to promote the warburg effect and tumor growth. *Sci Signal* (2009) 2:ra73. doi: 10.1126/scisignal.2000431
30. Wang H-J, Hsieh Y-J, Cheng W-C, Lin C-P, Lin Y-S, Yang S-F, et al. JMJD5 regulates PKM2 nuclear translocation and reprograms HIF-1 α -mediated glucose metabolism. *Proc Natl Acad Sci USA* (2014) 111:279–84. doi: 10.1073/pnas.1311249111
31. Yang Y-C, Chien M-H, Liu H-Y, Chang Y-C, Chen C-K, Lee W-J, et al. Nuclear translocation of PKM2/AMPK complex sustains cancer stem cell populations under glucose restriction stress. *Cancer Lett* (2018) 421:28–40. doi: 10.1016/j.canlet.2018.01.075
32. Fan J, Hitosugi T, Chung T-W, Xie J, Ge Q, Gu T-L, et al. Tyrosine phosphorylation of lactate dehydrogenase is important for NADH/NAD⁺ redox homeostasis in cancer cells. *Mol Cell Biol* (2011) 31:4938–50. doi: 10.1128/MCB.06120-11
33. Wilde L, Roche M, Domingo-Vidal M, Tanson K, Philp N, Curry J, et al. Metabolic coupling and the reverse warburg effect in cancer: Implications for novel biomarker and anticancer agent development. *Semin Oncol* (2017) 44:198–203. doi: 10.1053/j.seminoncol.2017.10.004
34. Gu J, Wu M, Guo R, Yan K, Lei J, Gao N, et al. The architecture of the mammalian respirasome. *Nature* (2016) 537:639–43. doi: 10.1038/nature19359
35. Hood D, Zak R, Pette D. Chronic stimulation of rat skeletal muscle induces coordinate increases in mitochondrial and nuclear mRNAs of cytochrome c oxidase subunits. *Eur J Biochem* (1989) 179:275–80. doi: 10.1111/j.1432-1033.1989.tb14551.x
36. Renner K, Amberger A, Konwalinka G, Kofler R, Gnaiger E. Changes of mitochondrial respiration, mitochondrial content and cell size after induction of apoptosis in leukemia cells. *Biochim Biophys Acta* (2003) 1642:115–23. doi: 10.1016/s0167-4889(03)00105-8
37. Larsen S, Nielsen J, Neigaard Hansen C, Nielsen LB, Wibrand F, Stride N, et al. Biomarkers of mitochondrial content in skeletal muscle of healthy young human subjects. *J Physiol* (2012) 590:3349–60. doi: 10.1113/jphysiol.2012.230185
38. Youle JR, van der Bliek AM. Mitochondrial fission, fusion, and stress. *Science* (2012) 337:1062–5. doi: 10.1126/science.1219855
39. Giacomello M, Pyakurel A, Glytsou C, Scorrano L. The cell biology of mitochondrial membrane dynamics. *Nat Rev Mol Cell Biol* (2020) 21:204–24. doi: 10.1038/s41580-020-0210-7
40. Taguchi N, Ishihara N, Jofuku A, Oka T, Mihara K. Mitotic phosphorylation of dynamin-related GTPase Drp1 participates in mitochondrial fission. *J Biol Chem* (2007) 282:11521–29. doi: 10.1074/jbc.M607279200
41. Chang CR, Blackstone C. Cyclic AMP-dependent protein kinase phosphorylation of Drp1 regulates its GTPase activity and mitochondrial morphology. *J Biol Chem* (2007) 282:21583–7. doi: 10.1074/jbc.C700083200
42. Cribbs JT, Strack S. Reversible phosphorylation of Drp1 by cyclic AMP-dependent protein kinase and calcineurin regulates mitochondrial fission and cell death. *EMBO Rep* (2007) 8:939–44. doi: 10.1038/sj.embor.7401062
43. Losón OC, Song Z, Chen H, Chan DC. Fis1, mif, Mid49, and Mid51 mediate Drp1 recruitment in mitochondrial fission. *Mol Biol Cell* (2013) 24:659–67. doi: 10.1091/mbc.E12-10-0721
44. Yu R, Tong Liu T, Jin S-B, Ning C, Lendahl U, Nistér M, et al. MIEF1/2 function as adaptors to recruit Drp1 to mitochondria and regulate the association of Drp1 with mif. *Sci Rep* (2017) 7:880. doi: 10.1038/s41598-017-00853-x
45. Head B, Griparic L, Amiri M, Gandre-Babbe S, van der Bliek AM. Inducible proteolytic inactivation of OPA1 mediated by the OMA1 protease in mammalian cells. *J Cell Biol* (2009) 187:959–66. doi: 10.1083/jcb.200906083
46. Lafyatis R. Transforming growth factor β -at the centre of systemic sclerosis. *Nat Rev Rheumatol* (2014) 10:706–19. doi: 10.1038/nrrheum.2014.137
47. Inman GJ, Nicolás FJ, Callahan JF, Harling JD, Gaster LM, Reith AD, et al. SB-431542 is a potent and specific inhibitor of transforming growth factor- β superfamily type I activin receptor-like kinase (ALK) receptors ALK4, ALK5, and ALK7. *Mol Pharmacol* (2002) 62:65–74. doi: 10.1124/mol.62.1.65
48. Dakin LA, Block MH, Chen H, Code E, Dowling JE, Feng X, et al. Discovery of novel benzylidene-1,3-thiazolidine-2,4-diones as potent and selective inhibitors of the PIM-1, PIM-2, and PIM-3 protein kinases. *Bioorg Med Chem Lett* (2012) 22:4599–604. doi: 10.1016/j.bmcl.2012.05.098
49. Hickson I, Zhao Y, Richardson CJ, Green SJ, Martin NM, Orr AI, et al. Identification and characterization of a novel and specific inhibitor of the ataxia-telangiectasia mutated kinase ATM. *Cancer Res* (2004) 64:9152–59. doi: 10.1158/0008-5472.CAN-04-2727
50. Laping NJ, Grygielko E, Mathur A, Butter S, Bomberger J, Tweed C, et al. Inhibition of transforming growth factor (TGF)- β 1-induced extracellular matrix with a novel inhibitor of the TGF- β type I receptor kinase activity: SB-431542. *Mol Pharmacol* (2002) 62:58–64. doi: 10.1124/mol.62.1.58
51. Li Y, Yang D-Q. The ATM inhibitor KU-55933 suppresses cell proliferation and induces apoptosis by blocking akt in cancer cells with overactivated akt. *Mol Cancer Ther* (2010) 9:113–25. doi: 10.1158/1535-7163.MCT-08-1189
52. Kreuz S, Holmes KB, Tooze RM, Lefevre PF. Loss of PIM2 enhances the anti-proliferative effect of the pan-PIM kinase inhibitor AZD1208 in non-Hodgkin lymphomas. *Mol Cancer* (2015) 14:205. doi: 10.1186/s12943-015-0477-z
53. Zhu H, Chen W, Liu D, Luo H. The role of metabolism in the pathogenesis of systemic sclerosis. *Metabolism* (2019) 93:44–51. doi: 10.1016/j.metabol.2018.12.004
54. O'Reilly S. Metabolic perturbations in systemic sclerosis. *Curr Opin Rheumatol* (2022) 34:91–4. doi: 10.1097/BOR.0000000000000824
55. Chang CR, Blackstone C. Dynamic regulation of mitochondrial fission through modification of the dynamin-related protein Drp1. *Ann N Y Acad Sci* (2010) 1201:34–9. doi: 10.1111/j.1749-6632.2010.05629.x
56. Atkins K, Dasgupta A, Chen K-H, Mewburn J, Archer SL. The role of Drp1 adaptor proteins Mid49 and Mid51 in mitochondrial fission: implications for human disease. *Clin Sci (Lond)* (2016) 130:1861–74. doi: 10.1042/CS20160030
57. Yu R, Lendahl U, Nistér M, Zhao J. Regulation of mammalian mitochondrial dynamics: Opportunities and challenges. *Front Endocrinol* (2020) 11:374. doi: 10.3389/fendo.2020.00374
58. Pham TX, Lee J, Jiazhen Guan J, Caporarello N, Meridew JA, Jones DL, et al. Transcriptional analysis of lung fibroblasts identifies PIM1 signaling as a driver of

aging-associated persistent fibrosis. *JCI Insight* (2022) 7:e153672. doi: 10.1172/jci.insight.153672

59. Daugherty EK, Balmus G, Al Saei A, Moore ES, Abi Abdallah D, Rogers AB, et al. The DNA damage checkpoint protein ATM promotes hepatocellular apoptosis and fibrosis in a mouse model of non-alcoholic fatty liver disease. *Cell Cycle* (2012) 11:1918–28. doi: 10.4161/cc.20259
60. Henderson J, Duffy L, Stratton R, Ford D, O'Reilly S, Henderson J, et al. Metabolic reprogramming of glycolysis and glutamine metabolism are key events in myofibroblast transition in systemic sclerosis pathogenesis. *J Cell Mol Med* (2020) 24:14026–38. doi: 10.1111/jcmm.16013
61. Bernard K, Logsdon NJ, Ravi S, Xie N, Persons BP, Rangarajan S, et al. Metabolic reprogramming is required for myofibroblast contractility and differentiation. *J Biol Chem* (2015) 290:25427–38. doi: 10.1074/jbc.M115.646984
62. Bernard K, Logsdon NJ, Benavides GA, Sanders Y, Jianhua Zhang J, Darley-Usmar VM, et al. Glutaminolysis is required for transforming growth factor- β 1-induced myofibroblast differentiation and activation. *J Biol Chem* (2018) 293:1218–28. doi: 10.1074/jbc.RA117.000444
63. Bates J, Vijayakumar A, Ghoshal S, Marchand B, Yi S, Kornyejev D, et al. Acetyl-CoA carboxylase inhibition disrupts metabolic reprogramming during hepatic stellate cell activation. *J Hepatol* (2020) 73:896–905. doi: 10.1016/j.jhep.2020.04.037
64. Negmadjanov U, Godic Z, Rizvi F, Emelyanova L, Ross G, Richards J, et al. TGF- β 1-mediated differentiation of fibroblasts is associated with increased mitochondrial content and cellular respiration. *PLoS One* (2015) 10:e0123046. doi: 10.1371/journal.pone.0123046
65. Sun Q, Fang L, Tang X, Lu S, Tamm M, Stolz D, et al. TGF- β upregulated mitochondria mass through the SMAD2/3 \rightarrow C/EBP β \rightarrow PRMT1 signal pathway in primary human lung fibroblasts. *J Immunol* (2019) 202:37–47. doi: 10.4049/jimmunol.1800782
66. Selvarajah B, Azuelos I, Anastasiou D, Chambers RC. Fibrometabolism—an emerging therapeutic frontier in pulmonary fibrosis. *Sci Signal* (2021) 14:eaay1027. doi: 10.1126/scisignal.aay1027
67. Higo H, Ohashi K, Tomida S, Okawa S, Yamamoto H, Sugimoto S, et al. Identification of targetable kinases in idiopathic pulmonary fibrosis. *Respir Res* (2022) 23:20. doi: 10.1186/s12931-022-01940-y